Journal of Aircraft, Log Number : C10913

Experimental and Numerical Investigation of 65-deg Delta and 65/40-deg Double-Delta Wings

Ahmad Z. Al-Garni[*], Farooq Saeed[†] and Abdullah M. Al-Garni[‡]
King Fahd University of Petroleum and Minerals, Dhahran 31261, Saudi Arabia

In this study, an experimental and numerical investigation was carried out to obtain lift, drag, and pitching moment data on 65-deg delta and 65/40-deg double-delta wings. The experimental tests were conducted at the KFUPM low-speed wind tunnel facility whereas the numerical tests were performed using the commercial CFD software FLUENT. Results from both experiments and numerical predictions were compared to other experimental data found in literature as well as to the theory of Polhamus. The results of comparison of surface pressure coefficient distribution and vortex breakdown location show good agreement with experiments. Overall the comparison of result shows good agreement between different experimental studies as well as good agreement with the CFD predictions and the theoretical calculations.

Nomenclature

A	=	aspect ratio
b	=	wing span, m
C_D	=	wing drag coefficient
C_{D0}	=	profile drag coefficient
C_L	=	wing lift coefficient
C_N	=	normal force coefficient
C_T	=	thrust force coefficient
c	=	chord, m
c_p	=	pressure coefficient
c_r	=	root chord, m
p	=	pressure, N/m^2
q	=	dynamic pressure, N/m^2
Re_c	=	chord Reynolds number, $\rho Vc/\mu$
S	=	wing area, m^2
s	=	semi-span length, m
T	=	temperature, K
t	=	thickness, m
V	=	velocity, m/s
y	=	spanwise direction, m

Symbols

α	=	angle of attack, deg
Λ	=	sweep angle, deg
μ	=	viscosity, m^2/s
ρ	=	density, kg/m^3

I. Introduction

In a steady flow, the lift of a two-dimensional airfoil is contributed mainly by the leading edge suction peak. The lift increases with increasing angle of attack until the stall angle is reached. The separation on the upper surface will then reduce the leading edge suction peak causing the lift to drop. The static stall angle for a two-dimensional airfoil is about 10-15 degrees. The lift producing mechanism of a delta wing is somewhat different. The leading edge suction peak predicted by potential theory does not exist.[1] Instead two smooth suction peaks are seen to exist inward of the leading edges. These peaks are produced by a pair of stationary leading edge vortices formed by separation flow on the low-pressure side of the wing. Therefore, the lift on a delta wing is created by the separated vortical structures rather than by the attached flow over a convex surface. The lift keeps increasing with α until the leading edge vortex breaks down at an angle of about 30 degrees or more. The flow over a double-delta or straked-

[*] Professor and Chairman, Aerospace Engineering Department. AIAA Senior Member.
[†] Assistant Professor, Aerospace Engineering Department. AIAA Life Member.
[‡] Assistant Professor, Aerospace Engineering Department. AIAA Member.

delta wing is also found to be similar to that over the delta wing. Hence, delta and double-delta wings provide increased lift at high angles of attack.

Recent technological advances stress the need of high-lift and low drag forces in a wide range of angles of attack specifically in regards to advanced fighter aircraft in order to maintain their superiority through superior maneuverability. Since the maximum lift of a two-dimensional airfoil is typically obtained at 10-15 degrees angle of attack beyond which the airfoil stalls, one way to enhance performance of fighter aircrafts at high angle of attack is the use of delta or double-delta wings. As flow separates along the leading edges of a delta wing at non-zero angle of attack, vertical flow results into leading edge vortices (Fig. 1).[2] These vortices produce a very low pressure region and can account for up to 30% of the total lift at moderate angles of attack.[3] For example; a 70-deg delta wing continues to increase its lift up to an angle of attack of about 40 degrees. Unfortunately, there are limits to the benefits produced by the delta/double-delta wing vortices. As the angle of attack is increased further, there is a sudden change in the vortex flow-field when the core and structure of the vortex breaks down. Puckett and Stewart[4] used a combination of source distribution and conical flow theory to investigate the flow about delta- and arrow-shaped planforms. Cases studied included subsonic and/or supersonic leading and trailing edges with double wedge airfoil sections. Polhamus[5, 6] developed the leading edge suction analogy. The correlation developed by Polhamus applies to thin wings having neither camber nor twist. Furthermore, the method is applicable to wings for which the leading edges are of sufficient sharpness that separation is fixed at the leading edge.

Some of the more recent investigations focus on the study of the processes underlying vortex breakdown through flow visualization experiments,[6-13] theoretical/semi-empirical[14-18] and computational fluid dynamics (CFD)[19-27] based prediction methods involving delta and/or double-delta wings. One of the objectives of this study is to successfully and accurately model the 65-deg delta and 65/40-deg double-delta wings so as to obtain reliable prediction of aerodynamic loads at high angles of attack. Thus, the first task of the study was to successfully and reliable obtain experimental aerodynamic performance data on the 65-deg delta and 65/40-deg double-delta model wings. The data was then compared with other experimental data found in literature. Once the validity of the experimental data is established, the experimental data can then be used to validate in-house computational study and thus ascertain the maximum possible benefit that can be obtained through operation at high angles of attack in terms of maneuverability at high angles of attack. Future studies can then provide an insight into the location of leading-edge vortices as a function of leading-edge sweep and other test conditions. This information will be vital for a parallel in-house study to numerically investigate the effect of spanwise suction on delta-wing aerodynamics, in general, and vortex interaction and breakdown, in particular. Thus, the on-going effort will provide useful information regarding the best location for spanwise suction for a given delta/double-delta wing geometry and flight conditions in order to investigate the effect of suction in further delaying the vortex breakdown process and greatly enhancing the vortex lift envelop.

In the sections that follow, the paper presents some brief details of the in-house experimental setup, the numerical model and the CFD tool used for the analysis, a results and discussion section highlighting some of the key results, experimental as well as numerical, of this investigation of the 65-deg delta and 65/40-deg double delta wings, followed by some brief conclusions.

II. Experimental Facility

Experiments on a 65-deg delta and a 65/40-deg double-delta wings were conducted in the wind tunnel facility at KFUPM. A brief description of the models and the experimental setup is given below.

A. Model Description

The delta and double-delta wing models used in the experiments are shown in Fig. 2. Both the wings were made up of smooth, flat aluminum plate sections with beveled leading edges and rectangular trailing edges. The key features of the two wings are listed in Table 1. The dimensions of the delta wing model are as follows: leading edge sweep angle Λ_{le} = 65 degrees, root chord c = 0.3 m, wing span b = 0.2798 m, wing area $S = cb/2$ = 0.04197 m^2, aspect ratio $AR = b^2/S$ = 1.865, bevel angle = 8.5 degree and thickness t = 0.01 m. The dimensions of the double-delta wing model are as follows: in-board leading edge sweep Λ_i = 65 degrees, out-board leading edge sweep angle Λ_o = 40 degrees, root chord c = 0.301 m, wing span b = 0.468 m, wing area $S = cb/2$ = 0.0539 m^2, aspect ratio $AR = b^2/S$ = 4.064, bevel angle = 8.5 degree and thickness t = 0.01 m.

B. Wind Tunnel Facility

Experiments were conducted at the low-speed blow-down wind tunnel of King Fahd University of Petroleum & Minerals (KFUPM), Dhahran, Saudi Arabia, which is of the open return type as shown in Fig. 3. The test section is rectangular and has dimensions of 0.8 m × 1.1 m and a length of 3 m. The maximum free-stream velocity in the empty test section is V = 35 m/s and the turbulence level is slightly less than 1%. The tunnel is operated continuously and a centrifugal blower is driven by a 15 kW electric motor.

C. Test Conditions

For the balance measurements, the free-stream dynamic pressure q was 100 N/m^2 and the free-stream velocity upstream of the model was about 13 m/s which gives a chord Reynolds number of $Re_c = 2.67 \times 10^5$ based on model centerline chord. The velocity was kept constant within ±2%. The temperature of the air was also constant at a value of T = 300 K within ±1%, and the atmospheric pressure $p = 1.008 \times 10^5$ N/m^2 within ±2%. The test conditions for the current investigation covered a range of angle of attack α from 0-40 degrees within ±0.5 degree.

D. Data Acquisition

The wing models were mounted on a Rollab six-component balance. The balance (Rollab model I6B312) is an internal six component strain gauge of a bending beam type, designed to measure the force and moment systems on wind tunnel models that are mounted on the fore end of the balance and fixed by means of a screw and key. The aft end of the balance is fixed to one of three alternative balance legs, which in turn are mounted on the vertical strut of the fully-automated attitude mechanism (ATM312). Each balance leg is provided with a clamping device in order to obtain three ranges of angles of attack (-8 to 32 degrees, 22 to 62 degrees, and 52 to 92 degrees). The balance is provided with six strain gauge (SG) bridges. The zero drift of the SG-bridges is compensated for changes in the temperature level. The Rollab balance is supplied with calibration matrix based on a second-degree mathematical model. Balance nominal loads, which can be exceeded in an emergency situation by 100% without any permanent deformation, are given in Table 2. A smart differential pressure transducer with an uncertainty error of ±1% was also used for measuring the dynamic pressure. The balance comes with very useful graphical user interface modules based on LabView software for various functionalities related to balance calibration, data acquisition, data processing (graphical and or text), hardware tests, etc., that help facilitate data acquisition, recording and post-processing.

III. Numerical Model

The second part of the current study involved numerical investigation of the aerodynamic loads on the 65-deg delta and 65/40-deg double-delta wings using FLUENT[28] (v6.0.20), a state-of-the-art commercial computational fluid dynamic (CFD) solver. FLUENT was used not only to obtain the aerodynamic loads on the numerical models but also to determine how closely it can be used to model the delta wing vortex dynamics. FLUENT can simulate a large variety of flow problems from subsonic to hypersonic, viscous and inviscid conditions. The geometry for the CFD analysis is modeled using the GAMBIT (v2.0.4) software associated with FLUENT. Different CFD problems require different mesh types, and GAMBIT provides a host of options in a single package, in that it allows various options for volume meshing 3D geometries that include structured/unstructured, hex/tetrahedral, boundary layer, and manual/automated meshing with control over grid clustering. Moreover, it can be used to mesh using automatic cell size distribution to correctly account for sharp curvatures, boundary layers, etc., using the size-function functionality. The choice of mesh is greatly dependent on the choice of turbulence model which in turn depends on considerations such as the physics to be modeled, the level of accuracy required, the available computational resources as well as time available for the study. In order to choose the most appropriate turbulence model, a basic understanding of the capabilities and limitation of the various turbulence models needs to be understood. A brief discussion of the various turbulence models available in FLUENT and the reasons for the choice of turbulence model considered in this study are given below. For details on the various turbulence models available in FLUENT, the reader should refer to the associated literature.

The most economical options (computational-wise) available in FLUENT are the different methods for the solution of the Reynolds-averaged Navier-Stokes (RANS) equations for the mean flow quantities, with all the scales of the turbulence being modeled. The RANS method utilizes the Boussinesq hypothesis to relate the Reynolds stresses to the mean velocity gradients in order to facilitate closure of the governing equations. The RANS approach is most commonly used for practical engineering problems and uses turbulence models such as Spalart-Allmaras,[29] k-ε,[30—33] and k-ω[34, 35] and their variants, to name a few.

The Spalart-Allmaras[29] model is a one-equation model that solves a modeled transport equation for the kinematic eddy (turbulent) viscosity in which it is not necessary to calculate a length scale related to the local shear layer thickness. Although, in its original form, the Spalart-Allmaras model is a low-Reynolds-number model and requires proper resolution of the viscous-affected region of the boundary layer. In FLUENT, however, the Spalart-Allmaras model has been incorporated to use wall functions when the mesh resolution is not sufficiently fine and relatively crude simulations on coarse meshes are to be performed where accurate turbulent flow computations are not critical. The k-ε,[30—33] and k-ω[34, 35] turbulence models and their variants, are a class of two-equation semi-empirical/empirical models that solve the model transport equations for the turbulence kinetic energy (k) and its dissipation rate (ε) or the specific dissipation rate (ω), which can also be considered as a ratio of k to ε, respectively. The k-ε turbulence model was primarily designed for turbulent core flows (i.e., the flow in the regions somewhat far from walls). To give due considerations to the effect of the presence of walls, the k-ω turbulence model suitable for wall-bounded flows, was developed. The standard k-ω[34] turbulence model includes modifications for low-Reynolds-number effects, compressibility, and shear flow spreading that predict free shear flow spreading rates that are in close agreement with measurements for far wakes, mixing layers, and plane, round, and radial jets, and is thus recommended[28] for wall-bounded flows and free shear flows. An improvement over the standard k-ω turbulence model is the shear- stress transport (SST) k-ω[35] turbulence model that incorporates a blending function designed to activate the standard k-ω turbulence models in the near-wall region and activate the k-ε turbulence model away from the surface. The SST k-ω[35] turbulence model also incorporates a damped cross-diffusion derivative term in the ω-equation along with a modified definition of turbulent viscosity to account for the transport of the turbulent shear stress.

Near the wall, variables have large gradients, and the momentum and other scalar transports occur most vigorously since the walls are the main source of mean vorticity and turbulence, therefore, accurate resolution of the flow in the near-wall region determines the fidelity of numerical solutions. The near wall region is generally considered to be composed of three layers. The innermost layer, known as the viscous sub-layer, is almost laminar in which the (molecular) viscosity plays a dominant role in momentum and heat or mass transfer. The outer layer, known as the fully-turbulent layer, is where turbulence plays a major role. There exists an interim region between the viscous sub-layer and the fully-turbulent layer where the effects of molecular viscosity and turbulence are equally important. In FLUENT, two approaches are available to model the near-wall region.

In one approach, the viscous sub-layer and the interim layer are not resolved. Instead, semi-empirical formulas called “wall functions” are used to bridge the viscous sub-layer and interim layer (viscosity-affected region) between the wall and the fully-turbulent region. The wall functions are a set of semi-empirical relations for (1) laws-of-the-wall for mean velocity and temperature (or other scalars), and (2) formulas for near-wall turbulent quantities, that in effect bridge the solution variables at the near-wall cells and the corresponding quantities on the wall. As mentioned earlier, the Spalart-Allmaras model in FLUENT has been modified to use in conjunction with the wall functions. The mesh guidelines for wall functions approach suggest that the distance from the wall at the wall-adjacent cell must be determined by considering the range of validity of the log-law. Since the log-law is valid for $y^+ > 30$ to 60, a value close to $y^+ = 30$ is recommended[28] and the boundary layer should contain a few cells.

In the other approach, known as the “near-wall modeling,” the turbulence models require the viscous sub-layer and interim layer to be resolved with a mesh all the way to the wall. The mesh guidelines for near-wall modeling approach suggest that the wall-adjacent cell must be on the order of $y^+ = 1$. A higher y^+ ($y^+ < 4$ or 5) is also acceptable so long it is well inside the viscous sub-layer. Moreover, there should be at least 10 ce11s within the viscosity affected region near the wall ($\mathrm{Re}_y < 200$) to be able to resolve the mean velocity and turbulent quantities in that region. For high-Reynolds number flows, the wall function approach substantially saves computational resources, because the viscous sub-layer and interim layer, in which the solution variables change most rapidly, do not need to be resolved. However, for the low Reynolds-number flows such as the case in this study, the viscous sub-layer and interim layer need to be resolved properly in order to obtain any meaningful results.

Initially, the use of wall functions approach on a mesh consisting of tetrahedral cells was constructed using the size function (automated grid generation) functionality available in GAMBIT. In this case, two different size functions were defined: one to capture the effects near the wall such that $y^+ = 30$ at the wall, and the second to economize the number of cells in the outer region that extended to the far field boundary. In this case, the one-equation Spalart-Allmaras turbulence model, with the vorticity-based production option, was used since it is able to

keep the resolution at a low level of complexity especially in regions of high velocity gradient. Moreover, the segregated and implicit formulation was used to iteratively arrive at a converged solution. FLUENT runs using the wall-function approach with size function functionality suggested that for accurate resolution of aerodynamic loads, a mesh size of 2-3 million cells is needed. Since such a computational resource was not available, the computational effort switched focused on the near wall modeling approach in which the wall-adjacent cell height was of the order of $y^+ < 3$ and at least 10 cells were used within the viscous sub-layer. Use of hexahedral cells and H-type topology were used to mesh the computational domain. Figure 4 shows the different views of the computational grid around the delta wing that was generated using GAMBIT. The regions above and below the delta and double-delta wing were meshed using the Cooper/Hex option whereas the rest of the regions were meshed using the Hex option. Of all the available turbulence models tested in the study (k-ε, standard k-ω and SST k-ω, etc.), the SST k-ω, model yielded aerodynamic loads (lift, drag coefficients) closer to the experimentally observed values. Initially the first-order upwind schemes were used in conjunction with a relaxation factors between 0.4-0.7. After 500-600 iterations, the second-order discretization schemes were employed. The convergence criteria used to monitor solution convergence was based on a two to three order-of-magnitude drop in the value of the residuals of mass, momentum, energy and turbulent viscosity.

Typical grids were of the order of 1.2 to 1.5 million cells. Due to coarse nature of initial grids, grid adaptation was typically carried out to achieve a value of y^+ below 3. Adapted grids typically consisted of approximately 20-30% more cells. The key features of the numerical models are listed in Table 3. The average CPU time per iteration listed in Table 3 is based on computations on a personal computer equipped with Pentium 4, single 2 GHz CPU, and 1 GB of RAM.

IV. Results and Discussion

This section gives a brief description of the main results of the study. Figure 5 shows a comparison of 65-deg delta wing lift coefficient based on theory (Polhamus), experiments (present study as well as others) and CFD (present study). The results of the theory were based on the theory proposed by Polhamus. The profile drag component was calculated using a panel method with an integral boundary layer calculation. In Fig. 6, a comparison of 65-deg delta wing induced drag coefficient based on theory, experiments (present study as well as others) and CFD (present study) is presented. Similarly, Fig. 7 shows a comparison of 65/40-deg double-delta wing lift coefficient based on theory, experiments (present study as well as others) and CFD (present study) whereas Fig. 8 shows a comparison of 65/40-deg double-delta wing drag coefficient based on theory, experiments and CFD. Figures 9 shows a comparison of 65-deg delta wing normal and tangential force coefficients based on theory (Polhamus) and experiment (current study). Finally, Fig. 10 shows a comparison of spanwise pressure coefficient distribution along the 50% chord predicted by FLUENT on the 65-deg delta wing of Ref. [36] at α = 30 deg. The vortex breakdown occurs nearly at 20% chord for the 65-deg delta wing at α = 30 deg which is also confirmed by experiments.[36, 37] Overall the comparison of result shows good agreement between different experimental studies as well as good agreement with the CFD predictions and the theoretical calculations.

V. Conclusion

In this study, an experimental and numerical investigation was carried out to obtain lift, drag, and pitching moment data on 65-deg delta and 65/40-deg double-delta wings. The experimental tests were conducted at the KFUPM low-speed wind tunnel facility whereas the numerical tests were performed using the commercial CFD software FLUENT. Results from both experiments and numerical predictions were compared to other experimental data found in literature as well as to the theory of Polhamus. The results of comparison of surface pressure coefficient distribution and vortex breakdown location show good agreement with experiments. Overall the comparison of result shows good agreement between different experimental studies as well as good agreement with the CFD predictions and the theoretical calculations.

Acknowledgments

The authors would like to acknowledge the support of King Fahd University of Petroleum & Minerals (KFUPM) for the Project No. FT040008 (Deanship of Scientific Research) in accomplishing this study.

References

[1]Jones, R.T. and Cohen, D., *High Speed Wing Theory*, Princeton University Press, Princeton, NJ, 1960.

[2]Polhamus, E., "A Concept of the Vertex Lift of Sharp-Edge Delta Wings Based on a Leading-Edge Suction Analogy", *NASA TN D-3767*, Dec. 1996.
[3]Puckett, A.E. and Stewart, H.J., "Aerodynamic Performance of Delta Wings at Supersonic Speeds", *Journal of the Aeronautical Sciences*, Vol. 14, No. 10, pp. 567-578, Oct. 1947.
[4]Polhamus, E.C., "Predictions of Vortex-Lift Characteristics by a Leading Edge Suction Analogy", *Journal of Aircraft*, Vol. 8, No. 4, Apr. 1971, pp. 193-199.
[5]Polhamus, E.C., "Charts for Predicting the Subsonic Vortex-Lift Characteristics of Arrow, Delta and Diamond Wings", *TN D-6243*, NASA, Apr. 1971.
[6]Gai, S.L., Roberts, M., Barker, A., Kleczaj, C., and Riley, A.J., "Vortex Interaction and Breakdown Over Double-Delta Wings," *Aeronautical Journal*, Vol. 108, No. 1079, Jan. 2004, pp. 27-34.
[7]Al-Garni, A.Z., Ahmed, S.A., Sahin, A.Z. and Al-Garni, A.M., "An Experimental Study of a 65-Degree Delta Wing with Different Pitching Rates", *Journal of Aircraft*, Vol. 47, No. 2, pp. 85-93, Jun. 2001.
[8]Hebbar, S.K., Platzer, M.F., and Fritzelas, A.E., "Reynolds Number Effects on the Vortical-Flow Structure Generated by a Double-Delta Wing," *Experiments in Fluids*, Vol. 28, No. 3, 2000, pp. 206-216.
[9]Hebbar, Sheshagiri K., Platzer, Max F., and Alkhozam, Abdullah M., "Experimental Study of Vortex Flow Control on Double-Delta Wings Using Fillets," *Journal of Aircraft*, Vol. 33, No. 4, July-Aug. 1996, pp. 743-751.
[10]Grismer, D. S., and Nelson, Robert C., "Double-Delta-Wing Aerodynamics for Pitching Motions With and Without Sideslip," *Journal of Aircraft*, Vol. 32, No. 6, Nov-Dec. 1995, pp. 1303-1311.
[11]Straka, William A. and Hemsch, Michael J., "Leading-Edge Vortex Breakdown for Wing Planforms with the Same Slenderness Ratio," *Journal of Aircraft*, Vol. 31, No. 3, May-June 1994, pp. 688-695.
[12]Verhaagen, N. G., "Visualization of the Vortex Flow Over Delta And Double-Delta Wings," Flow Visualization III, Proceedings of the Third International Symposium on Flow Visualization., Ann Arbor, MI, USA, Hemisphere Publishing Corp.,1985, pp. 652-658.
[13]Manor, D., and Wentz, William H. Jr., "Flow Over Double-Delta Wing and Wing Body at High Alpha," *Journal of Aircraft*, Vol. 22, No. 1, Jan. 1985, pp. 78-82.
[14]Ericsson, Lars E., "Vortex Characteristics of Pitching Double-Delta Wings," *Journal of Aircraft*, Vol. 36, No. 2, Mar-Apr. 1999, pp. 349-356.
[15]Lan, C. E., "Extensions of the Concept of Suction Analogy to Prediction of Vortex Lift Effect," NASA Conference Publication, 1986, pp. 65-84.
[16]Wood, Richard M. and Covell, Peter F., "Experimental and Theoretical Study of the Longitudinal Aerodynamic Characteristics of Delta and Double-Delta Wings at Mach Numbers of 1.60, 1.90, and 2.16," NASA Technical Paper, July 1985, 120p.
[17]Hoeijmakers, H. W. M., Vaatstra, W., and Verhaagen, N. G., "Vortex Flow Over Delta And Double-Delta Wings," *Journal of Aircraft*, Vol. 20, No. 9, Sep, 1983, pp. 825-832.
[18]Purvis, James W., "Analytical Prediction of Vortex Lift," *Journal of Aircraft*, Vol. 18, No. 4, Apr. 1981, pp. 225-230.
[19]Ekaterinaris, J.A., and Coutley, R.L., Schiff, L. B., and Platzer, M.F., "Numerical Investigation of High Incidence Flow Over a Double-Delta Wing," *Journal of Aircraft*, Vol. 32, No. 3, May-June 1995, pp. 457-463.
[20]Ekaterinaris, J.A. , "Effects of Spatial Order of Accuracy on the Computation of Vortical Flowfields," *AIAA Journal*, Vol. 32, No. 12, Dec. 1994, pp. 2471-2474.
[21]Hsu, C.-H., and Liu, C.H., "Investigation of Vortex Breakdown on Delta Wings Using Navier-Stokes Equations," *Fluid Dynamics Research*, Vol. 10, No. 4-6, Dec. 1992, pp. 399-408.
[22]Hsu, C.-H., and Liu, C.H., "Navier-Stokes Computation of Flow Around a Round-Edged Double-Delta Wing," *AIAA Journal*, Vol. 28, No. 6, June 1990, pp. 961-968.
[23]Yin, Xie-Yuan, Nan, X., and Deng, Guo-hua, "Numerical Simulation of Rolling Up of Leading/Trailing-Edge Vortex Sheets for Slender Wings," *AIAA Journal*, Vol. 27, No. 10, Oct. 1989, pp. 1313-1318.
[24]Fujii, K., Gavali, S., and Holst, T. L., "Evaluation of Navier-Stokes and Euler Solutions for Leading-Edge Separation Vortices," *International Journal for Numerical Methods in Fluids*, Vol. 8, No. 10, Oct. 1988, pp. 1319-1329.
[25]Hsu, C.-H., Hartwich, P.-M., and Liu, C.H., "Incompressible Navier-Stokes Computations for A Round-Edged Double-Delta Wing," *Journal of Aircraft*, Vol. 25, No. 8, Aug. 1988, pp. 675-676.
[26]Hsu, C.-H., Hartwich, P.-M., and Liu, C.H., "Computation of Vortical Interaction for a Sharp-Edged Double-Delta Wing," *Journal of Aircraft*, Vol. 25, No. 5, May 1988, pp. 442-447.
[27]Brennenstuhl, U., and Hummel, D., "Vortex Formation Over Double-Delta Wings," *Congress of the International Council of the Aeronautical Sciences*, ICAS Proceedings 1982, 13th Congress of the International Council of the Aeronautical Sciences/AIAA Aircraft Systems and Technology Conference, Seattle, WA, USA Vol. 2, 1982, pp. 1133-1146.
[28]FLUENT (v6.0.20) and GAMBIT (v2.0.4) software: www.fluent.com.
[29]Spalart, P., and Allmaras, S., "A One-Equation Turbulence Model for Aerodynamic Flows," AIAA Paper 92-0439, Jan. 1992.
[30]Launder, B. E., and Spalding, D. B., *Lectures in Mathematical Models of Turbulence*, Academic Press, London, England, 1972.
[31]Launder, B. E., and Spalding, D. B., "The Numerical Computation of Turbulent Flows," *Computer Methods in Applied Mechanics and Engineering*, Vol. 3, pp. 269-289, 1974.
[32]Yakhot, V., and Orszag, S. A., "Renormalization Group Analysis of Turbulence: I. Basic Theory," *Journal of Scientific Computing*, Vol. 1, No. 1, pp. 1-51, 1986.
[33]Shih, T.-H., Liou, W. W., Shabbir, A., Yang, Z., and Zhu, J., "A New k-ε Eddy-Viscosity Model for High Reynolds Number Turbulent Flows - Model Development and Validation," *Computers Fluids*, Vol. 24, No. 3, pp. 227-238, 1995.

[34]Wilcox, D. C., *Turbulence Modeling for CFD*, DCW Industries, Inc., La Canada, California, 1998.
[35]Menter, F. R., "Two-Equation Eddy-Viscosity Turbulence Models for Engineering Applications," *AIAA Journal*, Vol. 32, No. 8, pp. 1598-1605, August 1994.
[36]Verhaagen, N. G., and Jobe, C. E., "Wind-Tunnel Study on a 65-deg Delta Wing at Sideslip," *AIAA Journal of Aircraft*, Vol. 40, No. 2, March–April 2003. (Also AIAA Paper 2001-0691)
[37]Sohn, M. H., Lee, K. Y., and Chang, J. W., "Vortex Flow Visualization of a Yawed Delta Wing with Leading-Edge Extension," *AIAA Journal of Aircraft*, Vol. 41, No. 2, March–April 2004. (Also AIAA Paper 2002-3267)

Table 1: Key features of the wing models.

Parameter	Delta	Double-delta
Leading-edge/in-board sweep, Λ_{le} / Λ_i	65 deg	65 deg
Out-board sweep, Λ_o	-	40 deg
Root chord, c_r	0.3 m	0.301 m
Wing span, b	0.2798 m	0.468 m
Wing area, S	0.04197 m^2	0.05390 m^2
Aspect ratio, A	1.865	4.064
Thickness, t	0.01 m	0.01 m
Bevel angle	8.5 deg	8.5 deg

Table 2: Rollab sting balance nominal loads.

Force/Moment	Nominal Load
Normal force	150 N
Axial force	40 N
Side force	50 N
Pitching moment	5 N-m
Yawing moment	4 N-m
Rolling moment	3 N-m

Table 3: Key features of the numerical models.

Parameter	Delta	Double-delta
Grid size (hexahedral cells)	1,230,968	1,498,678
Process total memory (MBytes)	550	630
Reynolds number	0.267 million	0.267 million
Mach number	0.04	0.04
Average CPU time/iteration (sec)	40	68

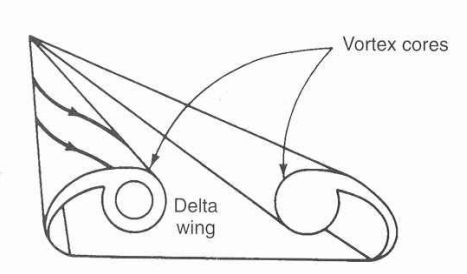

Figure 1: Vortex core development over a delta wing (Ref. 1).

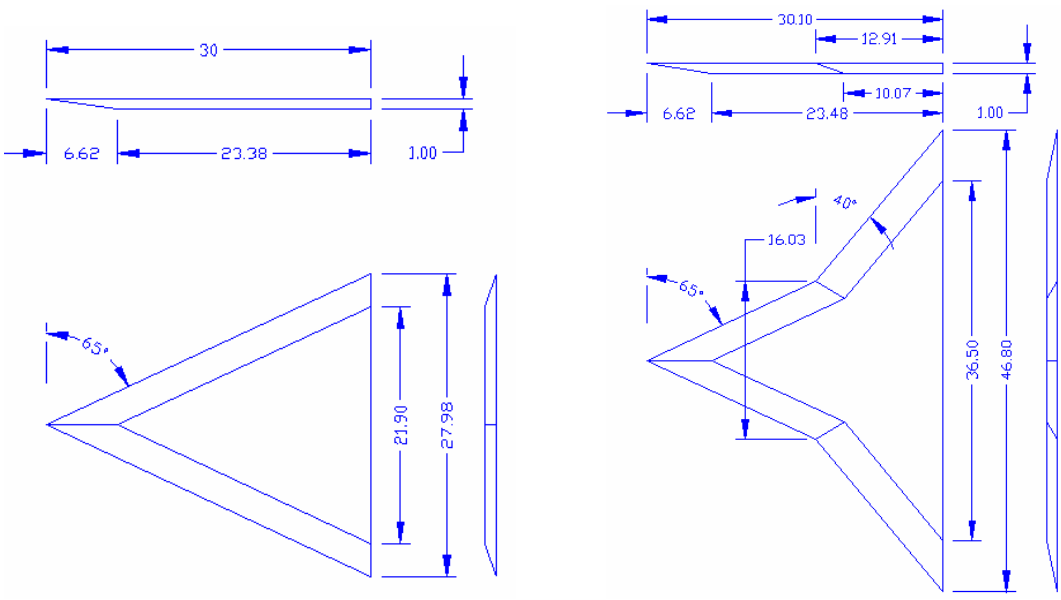

(a) **(b)**

Figure 2: Schematics of (a) 65-deg delta and (b) 65/40-deg double-delta wings.

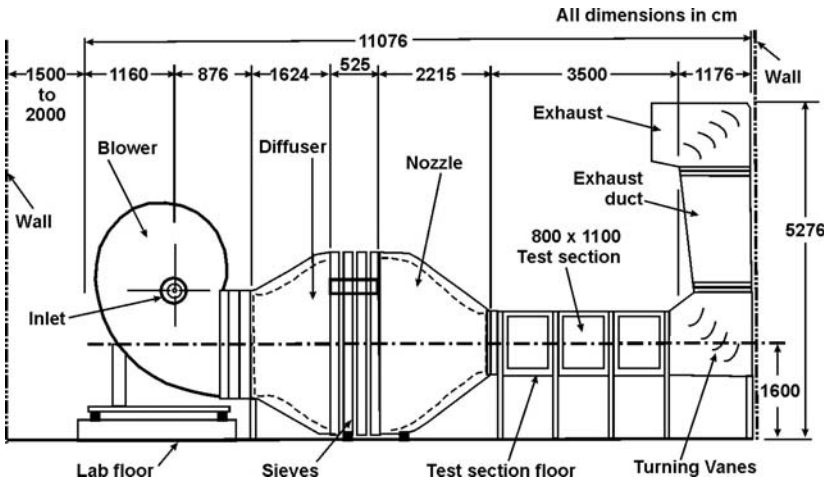

Figure 4: The open-circuit type wind tunnel test facility at KFUPM.

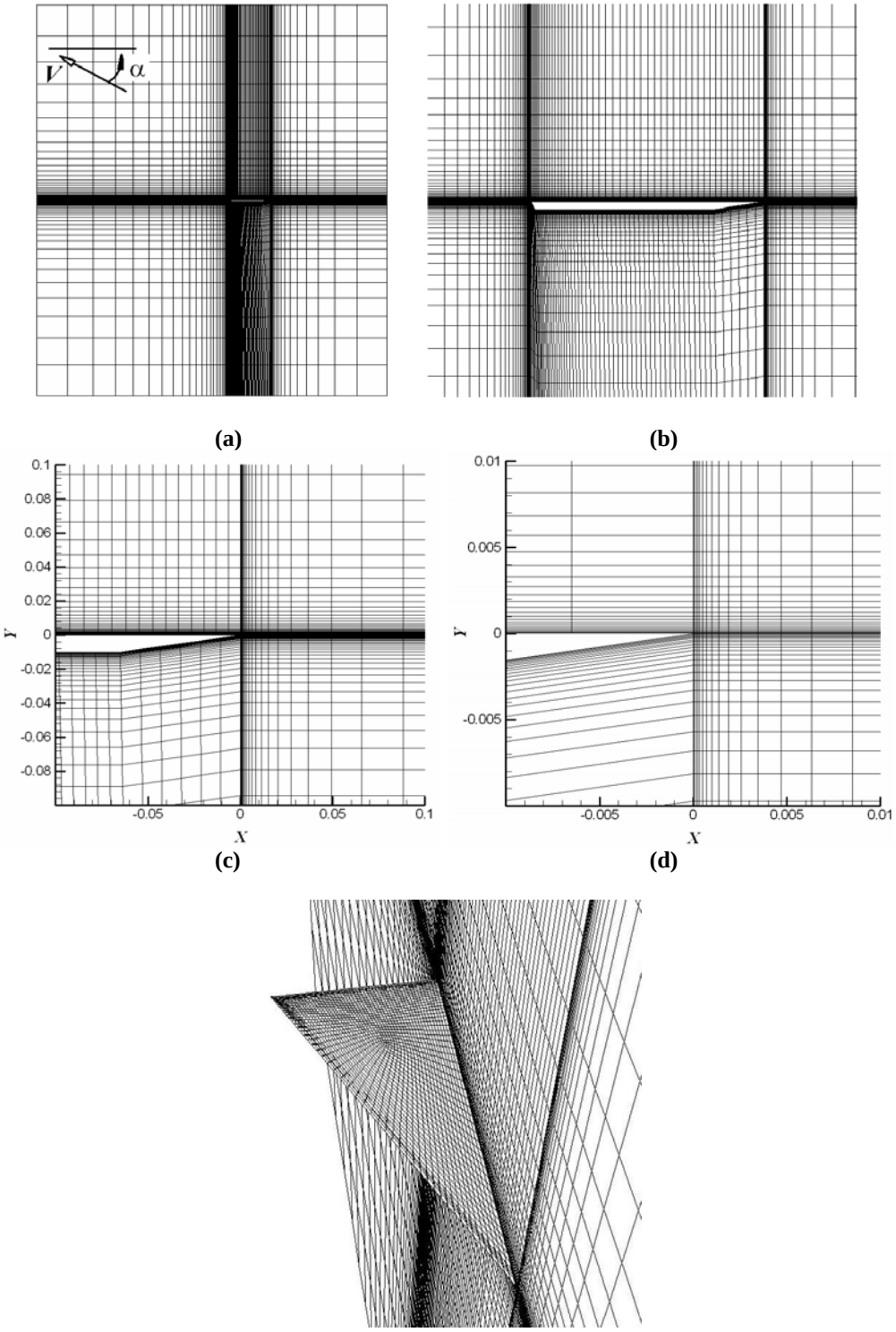

Figure 5: (a) Entire computational domain (side view), (b) Close-up view of the mesh around the delta wing (side view), (c) A close-up view of the mesh near the delta wing apex, (d) Further close-up view of the mesh near the delta wing apex, and (e) A perspective view of the 65-deg delta wing showing the lower surface mesh.

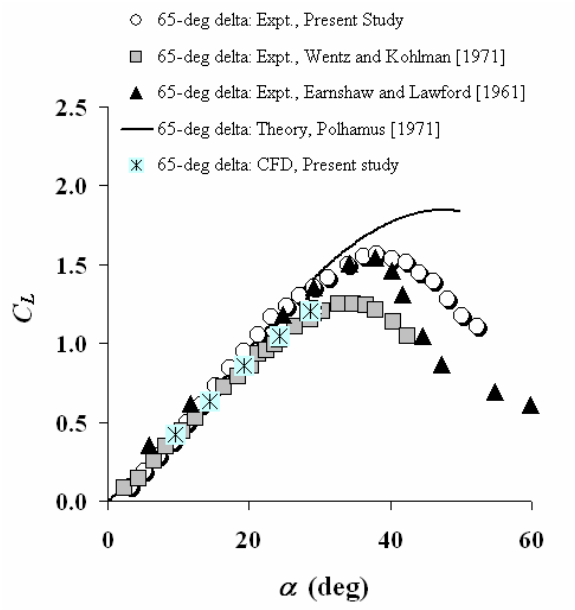

Figure 5: A comparison of 65-deg delta wing lift coefficient based on theory, experiments and CFD.

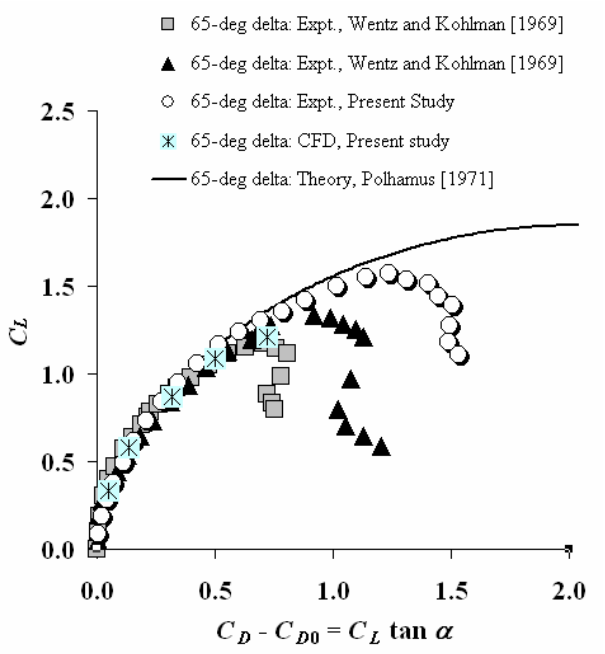

Figure 6: A comparison of 65-deg delta wing drag (induced) coefficient based on theory, experiments and CFD.

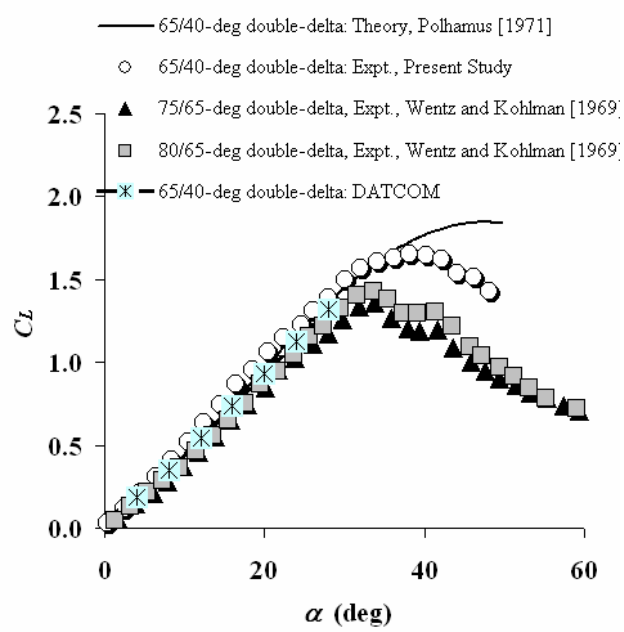

Figure 7: A comparison of 65/40-deg double-delta wing lift coefficient based on theory, experiments and CFD.

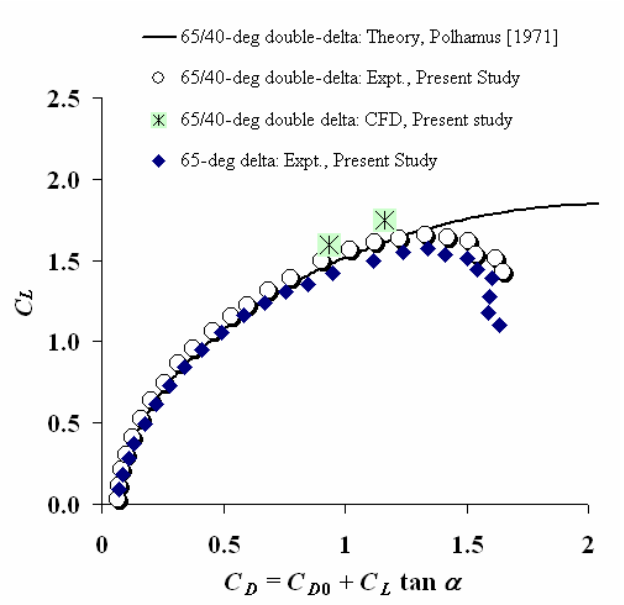

Figure 8: A comparison of 65/40-deg double-delta wing drag coefficient based on theory, experiments and CFD.

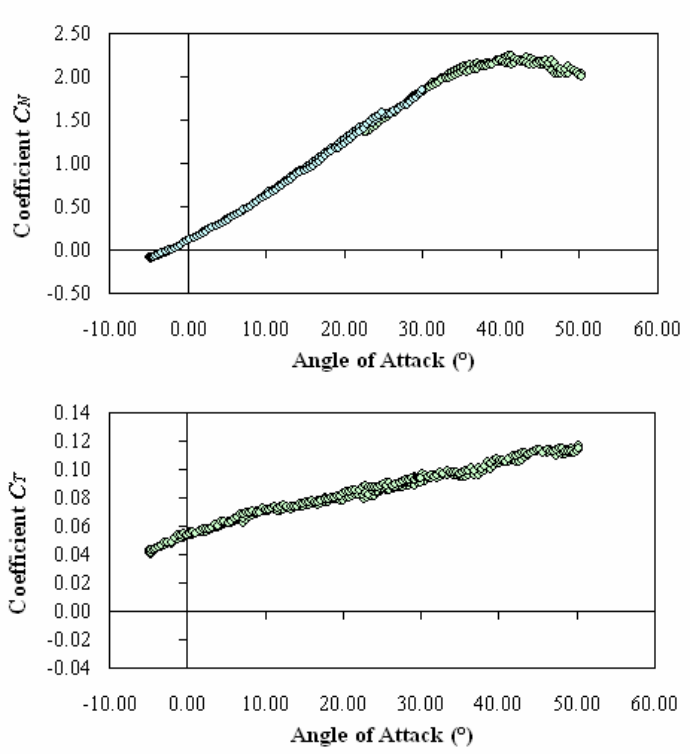

Figure 9: A comparison of 65-deg delta wing normal and tangential force coefficients based on theory (solid line) and experiments (circles).

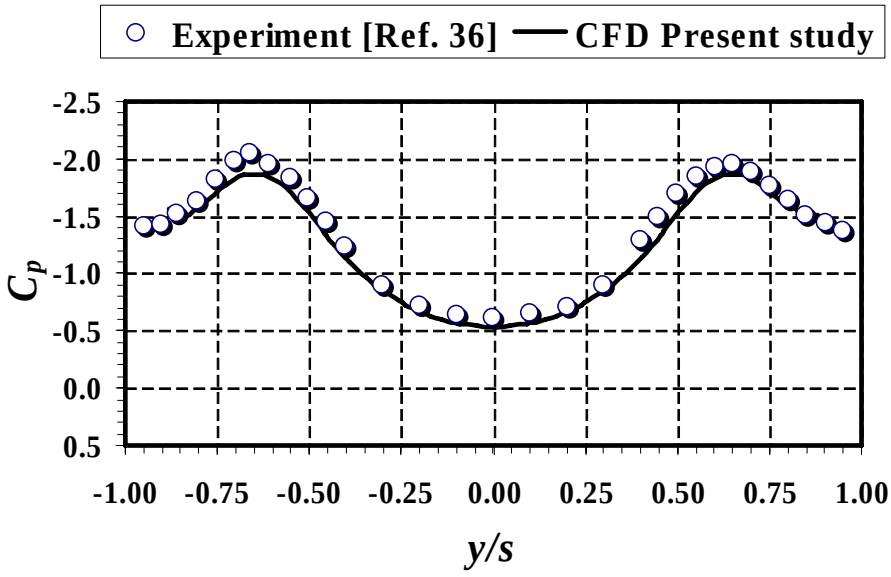

Figure 10: A comparison of spanwise pressure coefficient distribution along the 50% chord predicted by FLUENT on the 65-deg delta wing of Ref. [36] at α = 30 deg.